Laser-pulse compression by coherent control in a Doppler-broadened medium: Analytical and numerical studies

Roberto Buffa,[1] Stefano Cavalieri,[2] Emiliano Sali,[2] and Marco V. Tognetti[1]

[1]*Dipartimento di Fisica, Università di Siena, Via Roma 56, I-53100 Siena, Italy*

[2]*Dipartimento di Fisica, and European Laboratory for Nonlinear Spectroscopy, Università di Firenze, Via G. Sansone 1, I-50019 Sesto Fiorentino, Italy*

We have studied the temporal compression of laser pulses occurring in a scheme based on the coherent control peculiarities of electromagnetically induced transparency. This work extends earlier model studies, including the effect of Doppler broadening in a real hot medium. For definiteness and consistency of the atomic parameters employed, we have treated a scheme in argon. In this way, we establish a realistic model that enables us to predict quantitatively the performance of laser pulse compression experiments.

PACS number(s): 42.50.Gy, 42.65.Tg

I. INTRODUCTION

A well known commercial says that *power is nothing without control*. In effect it is a dream of any individual as well as of any society *to have things under control*. While in the real world this is often a frustrating task, in research laboratories the control of several chemical reactions and/or physical processes appears as an attainable, even though challenging, goal through the so-called coherent control.

One of the most interesting examples of coherent control processes is provided by electromagnetically-induced transparency (EIT) in which the optical properties of a material medium at wavelength λ_p can be controlled by an intense (control) laser field at a very different wavelength λ_c [1]. Since the first experimental demonstrations in atomic lead by Harris group at Stanford [2], EIT has been observed in various material media (atomic and molecular gases and solid crystals) and its possible applications have been widely discussed in many contexts: from the control of the absorption and of the group velocity [3] to the enhancement of optical nonlinearity [4], from light storage [5,6] to quantum memory [7–9]. Providing a complete account of previous work and an exhaustive list of references in a research paper is impossible, and the reader is then referred to the most recent review article on the subject [10].

More specifically, as far as this work is concerned, experimental evidence of the possibility to control the temporal shape of (probe) laser fields in the visible spectral region and in the microsecond temporal regime has been reported in cold atoms by Chien Liu *et al.* [11]. A theoretically study which discusses and explain how to exploit the peculiarities of EIT propagation dynamics to achieve coherent control of the temporal shaping of weak laser pulses has been also published [12]. So far this appears to be a unique technique in the far vacuum ultraviolet (VUV) or even extreme ultraviolet (XUV) spectral regions and may provide an important tool for nonlinear optics applications at very short wavelengths. Temporal compression appears as a special case of pulse shaping, and an experiment aimed to provide a first proof-of-principle demonstration in hot sodium atoms and in the visible spectral region is at present time under implementa-

tion in our laboratories [13]. Very recently, the approach of Ref. [12] has also been extended to the case of coherent population trapping (CPT) and the possibility of temporal shaping of intense laser pulses has been discussed [14].

The main goal of the present paper is to establish a realistic theoretical-numerical model that provides a deep understanding of the limits that can be achieved—and that enables to predict the performance attainable—from an experimental apparatus that exploits the temporal compression technique described in Ref. [12]. In effect, our previous analysis [12,15] assumed control laser intensities sufficiently large in order for the Doppler broadening to be safely neglected. However, for atomic transitions in the XUV, where Doppler broadening becomes particularly important, it is important to understand how the compression process works for decreasing intensities of the control laser and how the Doppler broadening affects the compression dynamics. Moreover, it is of evident interest to study how the compression process works at decreasing temporal duration of the probe laser pulse in order to identify a limit attainable with the proposed technique. This paper deals with such matters.

The paper is organized as follows. In Sec. II we introduce in a heuristic way the proposed technique and report the pertinent equations that have to be solved in order to quantitatively study the pulse compression dynamics. In Sec. III we review for completeness the analysis of Ref. [12], where Doppler broadening was ignored, and provide straightforward analytical expressions. In Sec. IV we report numerical calculations that allow to identify a threshold for the control laser intensity above which Doppler broadening can safely be ignored. In Sec. V we extend our analytical approach to include Doppler broadening and we provide straightforward analytical expressions that are in excellent agreement with the numerical results. Finally, in Sec. VI we extend our analysis to the case of short probe pulses.

II. THEORETICAL FRAMEWORK

Figure 1 shows a schematic diagram of the physical system at the basis of EIT: A three-level atom in interaction with
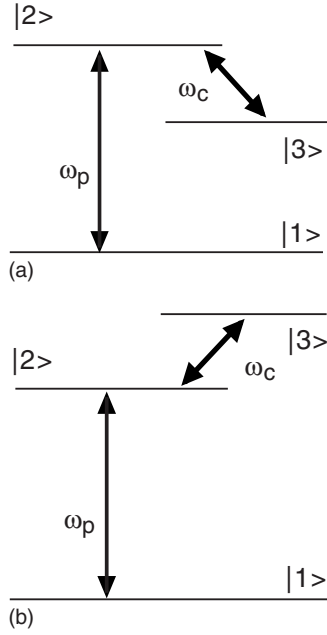
FIG. 1. Diagram of the three level scheme at the basis of EIT.

two laser pulses, of electric-field envelopes E_p (probe) and E_c (coupling), and frequencies ω_p and ω_c, resonant with the atomic transitions 1-2 and 2-3, respectively.

Figure 2 shows in a heuristic way the idea at the basis of the proposed technique. The laser pulses, propagating along the z axis, enter the cell of length L containing the medium of three-level atoms with the temporal overlapping shown in (a). The probe pulse (continuous line) experiences EIT and its propagation velocity v_p slows down to a value $v_p \ll c$ [10]. After some propagation in the cell, the coupling pulse (dashed line) overlaps the probe pulse as shown in (b). In this condition, different "points" of E_p experience different values of E_c and "travel" with different "propagation velocity," giving rise to a temporal reshaping of the probe pulse.

In a rigorous approach, using the slow varying envelope amplitude (SVEA) approximation in the Maxwell equations, leads to the following propagation equation for the electric-field envelopes E_p and E_c:

$$\left(\frac{\partial}{\partial z} + \frac{1}{c}\frac{\partial}{\partial t}\right)E_p = -iN\frac{\omega_p d_{12}}{\varepsilon_0 c}\langle\rho_{12}\rangle_v, \qquad (2.1a)$$

$$\left(\frac{\partial}{\partial z} + \frac{1}{c}\frac{\partial}{\partial t}\right)E_c = -iN\frac{\omega_c d_{23}}{\varepsilon_0 c}\langle\rho_{23}\rangle_v. \qquad (2.1b)$$

Here N is the density of the atomic sample, d_{12} and d_{23} are the electric-dipole moments of the transitions 1-2 and 2-3, respectively, and the coherences $\rho_{nm}(v)$ are averaged over the Maxwell-Doppler velocity distribution $f_D(v)$:
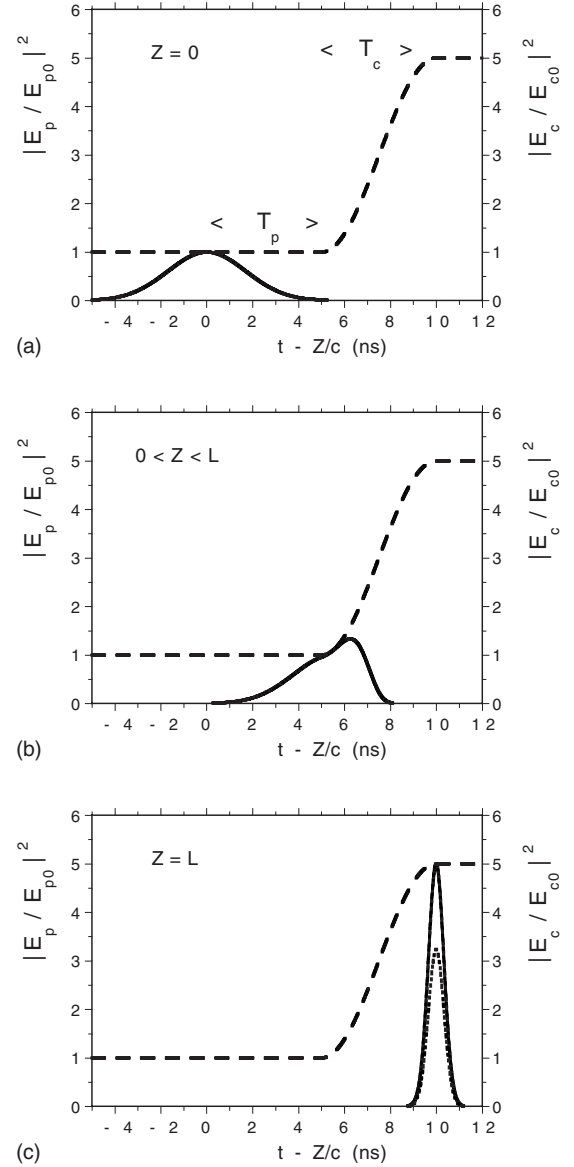

FIG. 2. The idea at the basis of the temporal compression process. In the framework moving at velocity c, the probe laser pulse *slips under* the coupling laser pulse along propagation in the atomic medium modified by EIT.

$$\langle\rho_{nm}\rangle_v = \int_{-\infty}^{+\infty}\rho_{nm}(v)f_D(v)dv. \qquad (2.2)$$

For the ladder (Ξ) scheme of Fig. 1(b), the coherences $\rho_{nm}(v)$ that appear in Eq. (2.2) satisfy the following Liouville equations:

$$\frac{d}{dt}\rho_{12} = i\Omega_p(\rho_{22} - \rho_{11}) - (i\Delta_p + \gamma_{12})\rho_{12} - i\Omega_c^*\rho_{13},$$

$$(2.3a)$$

$$\frac{d}{dt}\rho_{13} = -i\Omega_c\rho_{12} - [i(\Delta_p + \Delta_c) + \gamma_{13}]\rho_{13} + i\Omega_p\rho_{23},$$

$$(2.3b)$$

$$\frac{d}{dt}\rho_{23} = i\Omega_p^*\rho_{13} - (i\Delta_c + \gamma_{23})\rho_{23} + i\Omega_c(\rho_{33} - \rho_{22}),$$

$$(2.3c)$$

$$\frac{d}{dt}\rho_{11} = 2\,\mathrm{Im}(\Omega_p^*\rho_{12}) + \Gamma_{21}\rho_{22}, \qquad (2.3d)$$

$$\frac{d}{dt}\rho_{22} = -2\,\mathrm{Im}(\Omega_p^*\rho_{12}) + 2\,\mathrm{Im}(\Omega_c^*\rho_{23}) - \Gamma_{21}\rho_{22} + \Gamma_{32}\rho_{33},$$

$$(2.3e)$$

$$\frac{d}{dt}\rho_{33} = -2\,\mathrm{Im}(\Omega_c^*\rho_{23}) - \Gamma_{32}\rho_{33}, \qquad (2.3f)$$

where $\Omega_p = d_{12}E_p/2\hbar$ and $\Omega_c = d_{23}E_c/2\hbar$ are the Rabi couplings, $\Delta_p = (\omega_2 - \omega_1)(v/c)$ and $\Delta_c = (\omega_3 - \omega_2)(v/c)$ are detunings from resonance, Γ_{nm} are population decay rates, γ_{nm} represent all kind of dephasing rates, and the explicit dependence of the coherences $\rho_{nm}(v)$ on the velocity v of the atom has been dropped. For the lamda (Λ) scheme of Fig. 1(a), Ω_c should be replaced by Ω_c^* and $\Gamma_{32}\rho_{33}$ by $-\Gamma_{32}\rho_{22}$.

For a weak probe laser field E_p, to the first order perturbation theory in Ω_p, Eqs. (2.3) reduce to

$$\rho_{11} = 1, \quad \rho_{22} = \rho_{33} = \rho_{23} = 0,$$

$$\frac{d}{dt}\rho_{12} = -i\Omega_p - (i\Delta_p + \gamma_{12})\rho_{12} - i\Omega_c\rho_{13}, \qquad (2.4a)$$

$$\frac{d}{dt}\rho_{13} = -i\Omega_c\rho_{12} - [i(\Delta_p + \Delta_c) + \gamma_{13}]\rho_{13}, \qquad (2.4b)$$

where, since $\rho_{23} = 0$ and then

$$\left(\frac{\partial}{\partial z} + \frac{1}{c}\frac{\partial}{\partial t}\right)E_c = 0, \qquad (2.5)$$

Ω_c has been taken as real. Equations (2.4a) and (2.4b) apply in this form to both the schemes of Fig. 1.

III. STRONG-COUPLING REGIME: NEGLIGIBLE DOPPLER

To the first order in γ_{12}/Ω_c, γ_{13}/Ω_c, Δ_p/Ω_c, Δ_c/Ω_c, $\delta\omega_p/\Omega_c$, $\delta\omega_c/\Omega_c$ ($\delta\omega_p$ and $\delta\omega_c$ are the spectral widths of Ω_p and Ω_c, respectively) the solution of Eqs. (2.4a) and (2.4b) are given by

$$\rho_{12} = -\frac{i}{\Omega_c}\frac{d}{dt}\left(\frac{\Omega_p}{\Omega_c}\right) + [(\Delta_p + \Delta_c) - i\gamma_{13}]\frac{\Omega_p}{\Omega_c^2}, \qquad (3.1a)$$

$$\rho_{13} = -\frac{\Omega_p}{\Omega_c}. \qquad (3.1b)$$

The introduction of Eqs. (3.1a) in Eqs. (2.2) and (2.1a) provides

$$\frac{\partial}{\partial z}E_p + \frac{1}{c}\frac{\partial}{\partial t}E_p = -\frac{\kappa}{E_c}\left[\frac{\partial}{\partial t}\left(\frac{E_p}{E_c}\right) + \gamma_{13}\frac{E_p}{E_c}\right], \qquad (3.2)$$

with $\kappa = N(\hbar\omega_p/\varepsilon_0 c)(d_{12}/d_{23})^2$ and where, owing to Eq. (2.5),

$$E_c(z,t) = E_c(t - z/c). \qquad (3.3)$$

If, at $z=0$, the probe field E_p is overlapped by a flat region of the coupling field of value E_{c0} [see Fig. 2(a)], then the analytical solution of Eq. (3.2) is given by

$$E_p(z,t) = \frac{E_c}{E_{c0}} \times E_p\left(0, -\frac{\kappa}{E_{c0}^2}\xi\right)\exp\left[-\gamma_{13}\left(\frac{\kappa}{E_{c0}^2}\xi + t - z/c\right)\right], \qquad (3.4)$$

where $\xi(z,t) = z - \int_0^{t-z/c}(E_c^2/\kappa)d\tau$.

If we assume that the probe field at the cell output ($z = L$) is overlapped by a flat region of the coupling field of value nE_{c0} [see Fig. 2(c)], then Eq. (3.4) provides the following expression for the probe pulse intensity $I_p = E_p^2/2c\epsilon_0$

$$I_p(L,t) = n^2 I_p[0, n^2(t - t_L)]\exp\{-2\gamma_{13}[n^2(t_L - t) + t - L/c]\}, \qquad (3.5)$$

where t_L, defined implicitly through $L = \int_0^{t_L - L/c}(E_c^2/\kappa)d\tau$, is the arrival time of the probe pulse. For a negligible dephasing rate γ_{13}, Eq. (3.5) shows how the probe pulse, while preserving its functional shape, is temporally compressed by a factor n^2 and amplified by a factor n^2 [full curve in Fig. 2(c)]. However, for a not negligible dephasing rate γ_{13}, Eq. (3.5) shows an energy absorption of the probe pulse

$$\alpha = 1 - \int_{-\infty}^{+\infty} I_p(L,t)dt \Bigg/ \int_{-\infty}^{+\infty} I_p(0,t)dt. \qquad (3.6)$$

From Fig. 2(c), it appears that, in order to reach the full compression, one must have $\Delta t > \{[(n^2 + 1)/n^2]T_p + T_c\}$, where $\Delta t = t_L - L/c$ is the temporal delay accumulated by the probe pulse with respect the coupling pulse, $2T_p$ is the full temporal width of the probe pulse at the cell input, and T_c is the rise time between the two plateaus of the coupling pulse. When the temporal duration of the probe pulse at the cell output $2T_p/n^2$ is much shorter than the dephasing time $(2\gamma_{13})^{-1}$, the energy absorption α approaches the value

$$\alpha_0 = 1 - \exp\left[-2\gamma_{13}\left(\frac{n^2 + 1}{n^2}T_p + T_c\right)\right] \qquad (3.7)$$

[see dashed curve in Fig. 2(c)].

The main difference between the Ξ and the Λ schemes shown in Fig. 1 is contained in this result. The Λ scheme is the one that allows the use of a metastable final state, which in turns may lead to a coherence ρ_{13} with a negligible dephasing rate γ_{13}. On the other hand, if the goal is the control of XUV probe pulses by using a coupling field still in the visible spectral region, then it may not be possible to find a suitable high-energy metastable state and a loss in energy has to be taken into account.

IV. NUMERICAL STUDIES

Equations (3.4) and (3.5) are valid for qualitatively strong coupling fields. In order to quantitatively evaluate how intense the coupling field has to be, Eqs. (2.1a), (2.2), (2.4a), and (2.4b) have been numerically integrated using parallel computing techniques. In particular, the evaluation of the integral (2.2) requires the numerical integration of Eqs. (2.4a) and (2.4b) for several laser detunings depending on atomic velocity. Different integrations for different atomic velocities are independent from one another, and this makes the numerical code suitable for parallelization. The calculation was carried out using a code parallelized with the message passage interface (MPI) library running on a cluster linux with 256 available processors.

A central point of our technique is that the control laser field can be in the infrared or visible spectral region—where temporal shaping is already feasible from an experimental point of view—while the probe laser pulse could be in the VUV or even XUV spectral regions. Therefore, we studied a suitable ladder mixing scheme in argon where the ground state $|1\rangle = |(3s^2 3p^6)^1 S_0\rangle$ is coupled by a weak probe field at $\lambda_p = 2\pi c / \omega_p = 106.7$ nm to the excited state $|2\rangle = |(3s^2 3p^5)^2 P_{3/2}(4s)[3/2]^0, J=1\rangle$. This is coupled in turn to an upper state $|3\rangle = |(3s^2 3p^5)^2 P_{3/2}(4p)[1/2]^0, J=0\rangle$ by a strong coupling field at $\lambda_c = 2\pi c / \omega_c = 751.5$ nm. For such a scheme, the values of the FWHM Doppler broadening are $\delta\omega_{12} = 3.5 \times 10^{10}$ rad/s and $\delta\omega_{23} = 5.0 \times 10^9$ rad/s, respectively, as the values of the dephasing time are $(2\gamma_{12})^{-1} = 8.4$ ns and $(2\gamma_{13})^{-1} = 25$ ns.

A previous realistic numerical calculation was done for this scheme in the condition of negligible Doppler broadening [15]. We note that in that work a systematic error occurred in the computation of the absorption, which should be 36% and not completely negligible as reported there. Nevertheless, the main result of temporal compression by two orders of magnitude is unaffected by this error.

In the present calculations, the monomode probe pulse at the cell input $I_p(0,t)$ is taken as Gaussian with a FWHM temporal duration $\delta t_0 = 3$ ns ($\delta\omega_{p0} = 1.3 \times 10^9$ rad/s). The temporal behavior of the monomode coupling pulse features two flat regions of value I_{c0} and $n^2 I_{c0}$ ($n^2 = 10$) and a $\sin^2$-shaped interval of rise time $T_c = 1$ ns ($\delta\omega_c = 7 \times 10^8$ rad/s). The injection scheme at the cell input is that shown in Fig. 2(a) with an injection delay $T_p = \sqrt{2}\delta t_0 = 4.24$ ns while the NL product is chosen so that $\Delta t = t_L - L/c = [(n^2+1)/n^2]T_p + T_c = 5.67$ ns as shown in Fig. 2(c).
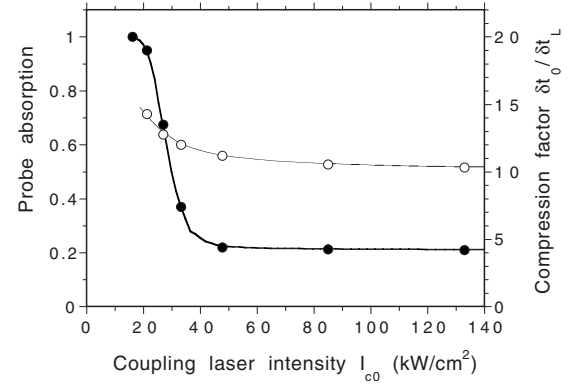

FIG. 3. Energy absorption (•) and compression factor (o) of a 3 ns probe laser pulse as a function of the coupling intensity I_{c0}. For each value of I_{c0} the NL product is chosen so that $\Delta t = 5.67$ ns. Solid lines reproduce analytical results.

The computed intensity of the probe pulse at the cell output $I_p(L,t)$ is then used to evaluate (i) the energy absorption α, Eq. (3.6), (ii) the compression factor $\delta t_0 / \delta t_L$ (δt_L is the FWHM temporal duration of the probe pulse at the cell output), and (iii) the adimensional quantity

$$\% = \frac{\int_{-\infty}^{+\infty} [I_p(L,t) - I_G(t)]^2 dt}{\int_{-\infty}^{+\infty} I_p^2(L,t) dt}, \qquad (4.1)$$

where $I_G(t)$ is a reference Gaussian function given by

$$I_G(t) = I_p(L,t_L) \exp[-4\ln(2)(t-t_L)^2 / \delta t_L^2] \qquad (4.2)$$

and t_L is the arrival time of the probe pulse. The quantity $\%$ Eq. (4.1) provides an evaluation of the temporal distortion experienced by the probe pulse upon propagation in the cell.

Dot points in Fig. 3 report the energy absorption α (•) and the compression factor $\delta t_0 / \delta t_L$ (o) as a function of the coupling laser intensity $I_{c0} = E_{c0}^2 / 2c\epsilon_0$. In all the range of values reported in Fig. 3, the value of $\%$ Eq. (4.1) remains below 10^{-3}, showing that the probe pulse preserves its Gaussian functional temporal shape. As expected by the analytical study presented in Sec. III, for sufficiently strong coupling intensities ($I_{c0} > 50$ kW cm^2), the probe pulse is temporally compressed by a factor $n^2 = 10$ with an energy absorption given by

$$\alpha_0 = 1 - \exp[-5.67/25] = 0.20.$$

For weaker coupling intensities ($I_{c0} < 50$ kW cm^2), we notice a compression factor even slightly larger than $n^2 = 10$. However, since in this range of coupling intensities the probe pulse is strongly absorbed, we deem this result to be of limited practical application.

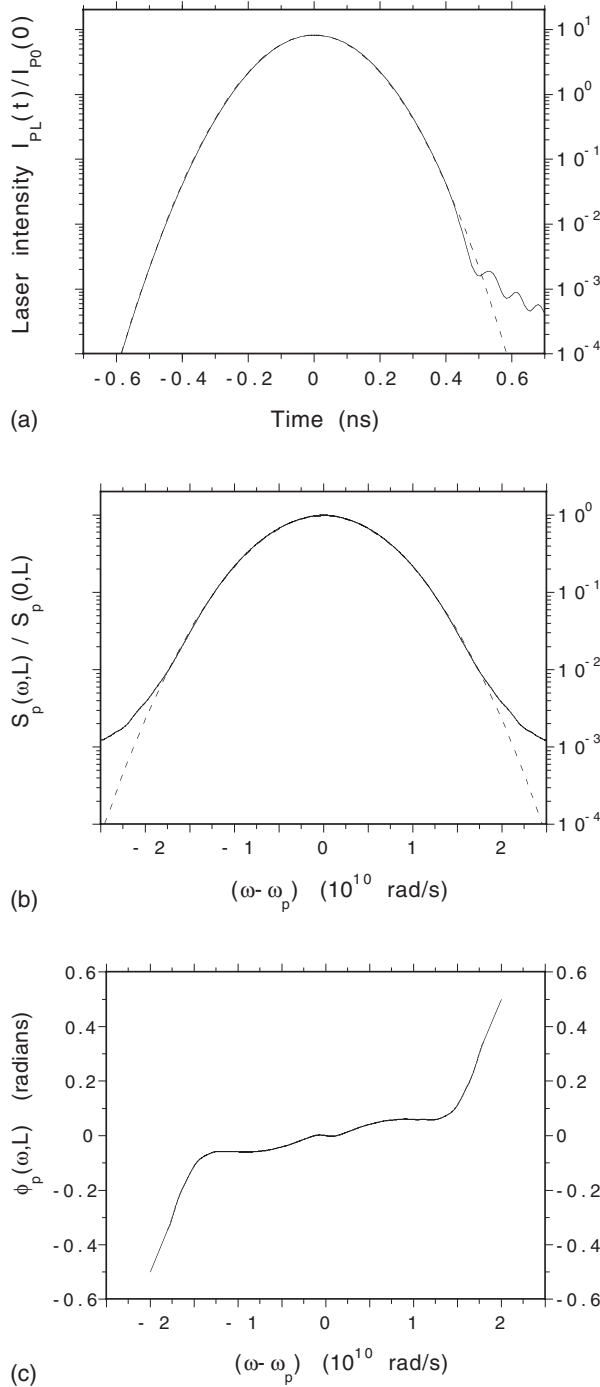As an example, in Fig. 4 the real quantities $I_p(L,t)$, $S_p(L,\omega)$, and $\phi_p(L,\omega)$ are reported, where

FIG. 4. Temporal behavior of (a) $I_p(L,t)$ and spectral behavior of (b) $S_p(L,\omega)$ and (c) $\phi_p(L,\omega)$ for a 3 ns input probe pulse with $I_{c0}=133$ kW/cm^2 and $NL=5.5\times10^{16}$ cm^{-2}. Dashed lines in (a) and (b) represent best Gaussian fits of FWHM equal to (a) 285 ps and (b) $\delta\omega_p=1.37\times10^{10}$ rad/s.

$$S_p(L,\omega)\exp[i\phi_p(L,\omega)]=\int_{-\infty}^{+\infty}E_p(L,t)\exp(i\omega t)dt \quad (4.3)$$

is the Fourier transform of $E_p(L,t)$ for $I_{c0}=133$ kW/cm^2. Dashed lines in (a) and (b) represent best Gaussian fits of FWHM equal to (a) $\delta t_L=285$ ps and (b) $\delta\omega_{pL}=1.37$

$\times10^{10}$ rad/s. The data show clearly that the compressed probe pulse remains monomode.

V. DOPPLER-BROADENED MEDIUM (INTERMEDIATE-COUPLING REGIME)

It is straightforward, even though tedious, to verify that, to the first order in $\delta\omega_p/\Omega_c$ and $\delta\omega_c/\Omega_c$, the solution of Eqs. (2.4a) and (2.4b) is given by

$$\rho_{12}=-\frac{\widetilde{\Delta}_{13}\Omega_p}{\widetilde{\Delta}_{12}\widetilde{\Delta}_{13}-\Omega_c^2}-i\frac{\Omega_c}{\widetilde{\Delta}_{12}\widetilde{\Delta}_{13}-\Omega_c^2}\frac{d}{dt}\left(\frac{\Omega_c\Omega_p}{\widetilde{\Delta}_{12}\widetilde{\Delta}_{13}-\Omega_c^2}\right)$$
$$-i\frac{\widetilde{\Delta}_{13}^2}{\widetilde{\Delta}_{12}\widetilde{\Delta}_{13}-\Omega_c^2}\frac{d}{dt}\left(\frac{\Omega_p}{\widetilde{\Delta}_{12}\widetilde{\Delta}_{13}-\Omega_c^2}\right), \quad (5.1a)$$

$$\rho_{13}=\frac{\Omega_c\Omega_p}{\widetilde{\Delta}_{12}\widetilde{\Delta}_{13}-\Omega_c^2}+i\frac{\widetilde{\Delta}_{13}\Omega_c}{\widetilde{\Delta}_{12}\widetilde{\Delta}_{13}-\Omega_c^2}\frac{d}{dt}\left(\frac{\Omega_p}{\widetilde{\Delta}_{12}\widetilde{\Delta}_{13}-\Omega_c^2}\right)$$
$$+i\frac{\widetilde{\Delta}_{12}}{\widetilde{\Delta}_{12}\widetilde{\Delta}_{13}-\Omega_c^2}\frac{d}{dt}\left(\frac{\Omega_c\Omega_p}{\widetilde{\Delta}_{12}\widetilde{\Delta}_{13}-\Omega_c^2}\right), \quad (5.1b)$$

with $\widetilde{\Delta}_{12}=\Delta_p-i\gamma_{12}$ and $\widetilde{\Delta}_{13}=\Delta_p+\Delta_c-i\gamma_{13}$.

The introduction of Eq. (5.1a) in Eqs. (2.2) and (2.1a) leads to

$$\frac{\partial}{\partial z}E_p+\frac{1}{c}\frac{\partial}{\partial t}E_p=\chi_1 E_p+\frac{1}{E_c}\frac{\partial}{\partial t}(\chi_2 E_p), \quad (5.2)$$

where, for resonant fields,

$$\chi_1=N\frac{\omega_p d_{12}^2}{2\hbar\varepsilon_0 c}\left[i\left\langle\frac{\widetilde{\Delta}_{13}}{\widetilde{\Delta}_{12}\widetilde{\Delta}_{13}-\Omega_c^2}\right\rangle_v\right.$$
$$+\frac{1}{\Omega_c}\left\langle\frac{\widetilde{\Delta}_{13}^2}{(\widetilde{\Delta}_{12}\widetilde{\Delta}_{13}-\Omega_c^2)^2}\right\rangle_v\frac{\partial\Omega_c}{\partial t}$$
$$\left.+\left\langle\frac{\widetilde{\Delta}_{13}^2+\widetilde{\Delta}_{12}\widetilde{\Delta}_{13}}{(\widetilde{\Delta}_{12}\widetilde{\Delta}_{13}-\Omega_c^2)^3}\right\rangle_v\frac{\partial\Omega_c^2}{\partial t}\right] \quad (5.3a)$$

and

$$\chi_2=-N\frac{\omega_p d_{12}^2}{d_{23}\varepsilon_0 c}\left\langle\frac{\widetilde{\Delta}_{13}^2+\Omega_c^2}{(\widetilde{\Delta}_{12}\widetilde{\Delta}_{13}-\Omega_c^2)^2}\right\rangle_v\Omega_c \quad (5.3b)$$

are real quantities.

If, at $z=0$, the probe field E_p is overlapped by a flat region of the coupling field of value E_{c0} [see Fig. 2(a)], then the analytical solution of Eq. (5.2) can be written as

$$E_p=\frac{\chi_{20}}{\chi_2}E_p\left(z=0;\frac{\chi_{20}}{E_{c0}}\xi\right)\exp\left[\chi_{10}\xi-\int_0^{t-z/c}\frac{\chi_1}{\chi_2}E_c d\tau\right]$$
$$(5.4)$$

with $\xi(z,t)=z+\int_0^{t-z/c}(E_c/\chi_2)d\tau$ and where

$$\chi_{10} = iN \frac{\omega_p d_{12}^2}{2\hbar\varepsilon_0 c} \left\langle \frac{\tilde{\Delta}_{13}}{\tilde{\Delta}_{12}\tilde{\Delta}_{13} - \Omega_{c0}^2} \right\rangle_v , \qquad (5.5a)$$

$$\chi_{20} = -N \frac{\omega_p d_{12}^2}{d_{23}\varepsilon_0 c} \left\langle \frac{\tilde{\Delta}_{13}^2 + \Omega_{c0}^2}{(\tilde{\Delta}_{12}\tilde{\Delta}_{13} - \Omega_{c0}^2)^2} \right\rangle_v \Omega_{c0}. \qquad (5.5b)$$

For a probe field E_p that, at $z=L$, is overlapped by a flat region of the coupling field of value nE_{c0} [see Fig. 2(c)], Eq. (5.4) provides the following expression for the probe intensity $I_p = E_p^2/2c\varepsilon_0$

$$I_p(L,t) = \left(\frac{\chi_{20}}{\chi_{2L}}\right)^2 I_p\left[z=0; n\frac{\chi_{20}}{\chi_{2L}}(t-t_L)\right]$$
$$\times \exp\left[2nE_{c0}\frac{\chi_{10}-\chi_{1L}}{\chi_{2L}}(t-t_L) - 2\int_0^{t_L-L/c} \frac{\chi_1}{\chi_2}E_c d\tau\right],$$
$$(5.6)$$

where

$$\chi_{1L} = iN \frac{\omega_p d_{12}^2}{2\hbar\varepsilon_0 c} \left\langle \frac{\tilde{\Delta}_{13}}{\tilde{\Delta}_{12}\tilde{\Delta}_{13} - n^2\Omega_{c0}^2} \right\rangle_v , \qquad (5.7a)$$

$$\chi_{2L} = -N \frac{\omega_p d_{12}^2}{d_{23}\varepsilon_0 c} \left\langle \frac{\tilde{\Delta}_{13}^2 + n^2\Omega_{c0}^2}{(\tilde{\Delta}_{12}\tilde{\Delta}_{13} - n^2\Omega_{c0}^2)^2} \right\rangle_v n\Omega_{c0} \quad (5.7b)$$

and the arrival time t_L of the probe pulse is defined through

$$L + \int_0^{t_L-L/c} \frac{E_c}{\chi_2}d\tau = 0.$$

Extending the interpretation provided in Sec. III, one could say that Eq. (5.6) shows that the probe pulse is temporally compressed by a factor $n\chi_{20}/\chi_{2L}$ and, in the limit of short duration at the cell output, the energy absorption α approaches the value

$$\alpha_0 = 1 - \exp\left[-2\int_0^{\Delta t} \frac{\chi_1}{\chi_2}E_c d\tau\right], \qquad (5.8)$$

where $\Delta t = t_L - L/c$ is the temporal delay accumulated by the probe pulse with respect the coupling pulse. As a matter of fact, in the limit of large Ω_c (strong coupling field), Eq. (5.4) reduces to Eq. (3.4), Eq. (5.6) to Eq. (3.5), and Eq. (5.8) to Eq. (3.7).

Expression (5.6) can be used to obtain the energy absorption α, Eq. (3.6), the compression factor $\delta t_0/\delta t_L$ (δt_L is the FWHM temporal duration of the probe pulse at the cell output) and the adimensional quantity %, Eq. (4.1). The results obtained for the same conditions used in the numerical calculations of Sec. IV are reported for comparison in Fig. 3 in continuous lines.

The excellent agreement between the analytical and the numerical studies makes the interpretation of the results straightforward. During the compression process from $\delta t_0 = 3$ ns to $\delta t_L = 300$ ps, the value of $\delta\omega_p$ increases from $\delta\omega_{p0} = 1.3 \times 10^9$ rad/s to $\delta\omega_{pL} = 1.3 \times 10^{10}$ rad/s, while, even for the lowest value of I_{c0} of Fig. 3 (20 kW/cm²), Ω_c increases
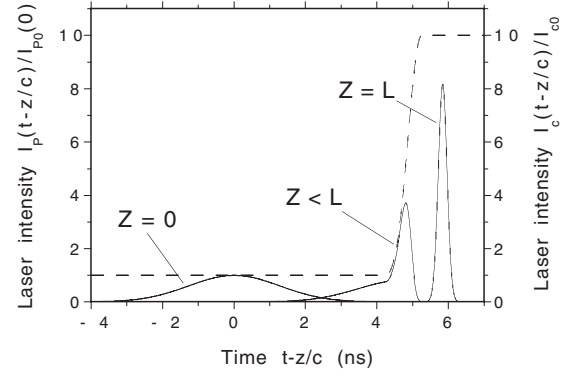

FIG. 5. Temporal evolution of $I_p(z,t)$ along the cell for a 3 ns input probe pulse with $I_{c0} = 85$ kW/cm² and $NL = 3.5 \times 10^{16}$ cm⁻². The curves obtained by numerical calculations and by analytical results cannot be resolved on the scale of the figure.

from $\Omega_{c0} = 4.4 \times 10^{10}$ rad/s to $\Omega_{cL} = 1.4 \times 10^{11}$ rad/s. Therefore, in all the range of values of Fig. 3, Ω_c is at any time more than one order of magnitude larger than $\delta\omega_p$ and $\delta\omega_c$, and the analytical expression (5.6), which is correct to the first order in $\delta\omega_p/\Omega_c$ and $\delta\omega_c/\Omega_c$, takes into account perfectly the effect of the Doppler broadening of the medium. This effect produces an extra absorption of the probe pulse that becomes negligible when $\Omega_{c0} > 2\delta\omega_{12}$. This allows us to set a threshold at $I_{c0} = 50$ kW/cm² (corresponding to $\Omega_{c0} = 2\delta\omega_{12}$) above which the Doppler effect can be safely ignored.

As an example, Fig. 5 reports the temporal evolution of the probe pulse along the cell for $I_{c0} = 85$ kW/cm². The curves obtained by numerical calculations and by Eq. (5.6) cannot be resolved on the scale of the figure.

VI. SHORT PROBE PULSE

In a ideal experiment, the probe pulse compressed in a first cell from 3 ns to 300 ps can be further compressed in a second cell using the same control pulse. We have then repeated the numerical calculations of Sec. III for a monomode Gaussian probe pulse at the cell input $I_p(0,t)$ with a FWHM temporal duration $\delta t_0 = 300$ ps ($\delta\omega_{p0} = 1.3 \times 10^{10}$ rad/s) and an injection delay $T_p = \sqrt{2}\delta t_0 = 424$ ps. For each value of I_{c0}, the NL product is chosen so that $\Delta t = t_L - L/c = 1.47$ ns. The results obtained are shown in Fig. 6 (dot points) and compared with the analytical results provided by the approach of Sec. V (solid lines)

For coupling intensities I_{c0} larger than 50 kW/cm², the probe absorption α (•) approaches the limit given by Eq. (3.5)

$$\alpha_0 = 1 - \exp[-1.47/25] = 0.06.$$

This result is in agreement with the evaluation of the previous section that set a threshold at $I_{c0} = 50$ kW/cm² above which the Doppler effect can be safely ignored. In this range of values the adimensional quantity % Eq. (4.1) remains below 10^{-3}, showing that the probe pulse preserves its Gaussian functional temporal shape. However, only for coupling
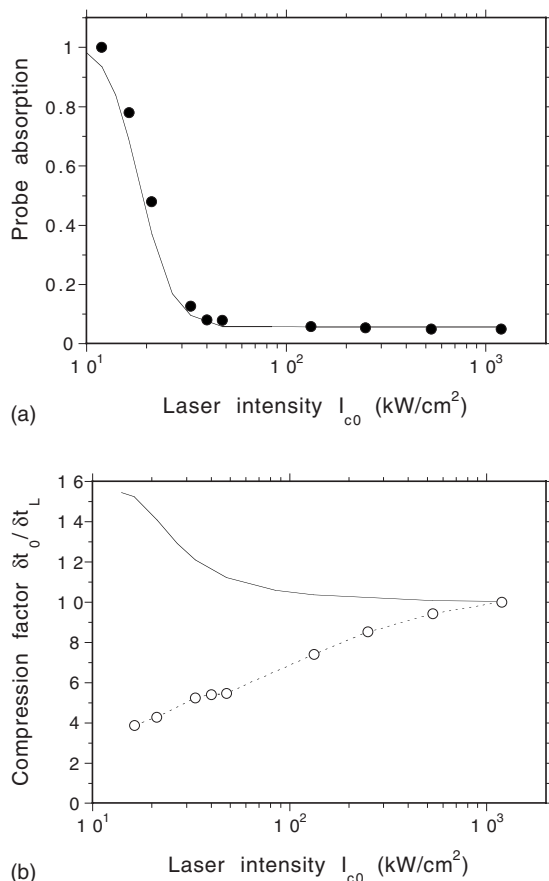
FIG. 6. Energy absorption (•) and compression factor (o) of a 300 ps probe laser pulse as a function of the coupling intensity I_{c0}. For each value of I_{c0} the NL product is chosen so that $\Delta t = 1.47$ ns. Solid lines reproduce analytical results.

FIG. 7. Evolution of (a) the probe pulse temporal duration δt and of (b) the ratio $\delta \omega_p / \Omega_c$ along propagation in the cell. (•) $I_{c0} = 133$ kW/cm², $NL = 4.7 \times 10^{16}$ cm⁻²; (o) $I_{c0} = 1.2$ MW/cm², $NL = 4.2 \times 10^{17}$ cm⁻². The ratios $\delta \omega_p / \Omega_c$ have been normalized to $\delta \omega_{p0} / \Omega_{c0}$ for an easy comparison.

intensities I_{c0} larger than 1 MW/cm², the full compression of 10 is reached.

These results show that the qualitative conditions $\Omega_c \gg \delta \omega_p$ and $\Omega_c \gg \delta \omega_{12}$ (both required in order to apply the strong-field analysis) lead to quantitatively different requirements at the cell input. In effect it has to be noted that, along propagation in the cell, the ratio $\delta \omega_{12} / \Omega_c$ decreases from $\delta \omega_{12} / \Omega_{c0}$ to $\delta \omega_{12} / n\Omega_{c0}$ whereas, according to Sec. III, the ratio $\delta \omega_p / \Omega_c$ increases from $\delta \omega_{p0} / \Omega_{c0}$ to $\delta \omega_{pL} / \Omega_{cL} = n\delta \omega_{p0} / \Omega_{c0}$. Therefore, while the condition $\Omega_{c0} > 2\delta \omega_{12}$ is sufficient to guarantee that $\Omega_c \gg \delta \omega_{12}$ everywhere in the cell, the condition $\Omega_{c0} \gg \delta \omega_{p0}$ must be much more stringent in order to guarantee that $\Omega_c \gg \delta \omega_p$ everywhere in the cell. Figure 7 shows how the pulse temporal duration δt and the ratio $\delta \omega_p / \Omega_c$ evolve along propagation in the cell for two different values of I_{c0}. The values of $\delta \omega_p / \Omega_c$ have been normalized to $\delta \omega_{p0} / \Omega_{c0}$ for an easy comparison. Dot points refer to results obtained by numerical calculations while the solid line is obtained by using the analytical Eq. (3.4).

For $I_{c0} = 1.2$ MW/cm² an effective compression process from $\delta t_0 = 300$ ps to $\delta t_L = 30$ ps takes place in which the Rabi frequency Ω_c varies from $\Omega_{c0} = 27\delta \omega_{p0}$ to $\Omega_{cL} = 8.5\delta \omega_{pL}$ with an excellent agreement between analytical and numerical calculations. For $I_{c0} = 133$ kW/cm² we have $\Omega_{c0} = 9\delta \omega_{p0}$, a value sufficient to provide an efficient probe compression in
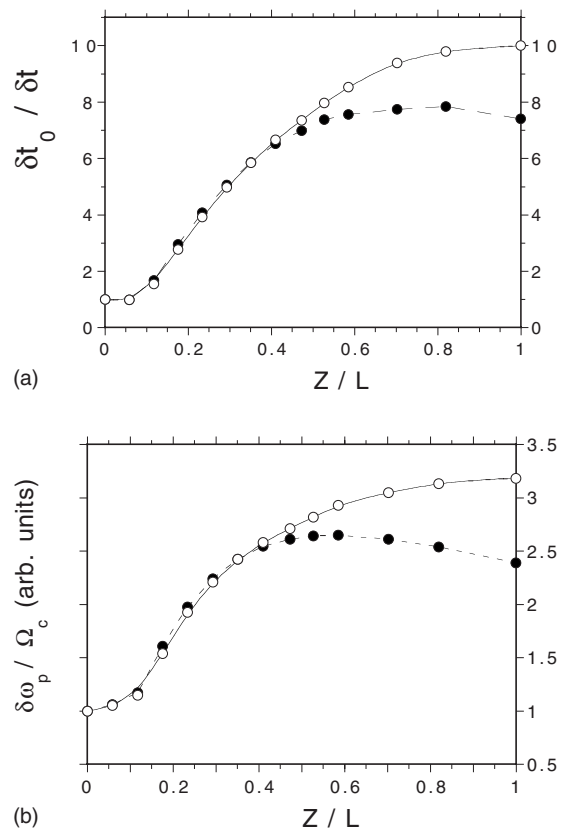
the first part of the cell. However, at $z/L = 0.4$ where $\Omega_c = 3.5\delta \omega_p$, the ratio $\delta \omega_p / \Omega_c$ shows a sudden saturation that eventually leads to the termination of the compression process. Nevertheless, it has to be noted that, even though unable to produce a compression of 10, the control pulse with $I_{c0} = 133$ kW/cm² provides a compression of 7.8 (corresponding to $\delta t_L = 38$ ps) for a reduced value of NL [$z/L = 0.8$ in Fig. 7(a)].

VII. CONCLUSIONS

We have presented analytical and numerical studies performed on a temporal compression scheme based on EIT. We have treated the case in which a far VUV probe laser pulse at $\lambda_p = 106.7$ nm is temporally compressed in a medium of argon atoms at room temperature from 3 ns to 30 ps in two steps in cascade. In both compression steps the Rabi frequency of the control field features two flat regions of value Ω_{c0} and $\Omega_{cL} = \sqrt{10}\Omega_{c0}$ and an interval of 1 ns risetime. Generally speaking, one could distinguish between two quite different regimes: Long or short probe pulse duration, depending on whether $\Omega_c > \delta \omega_{12} > \delta \omega_p$ or $\Omega_c > \delta \omega_p > \delta \omega_{12}$.

In the first compression step, from 3 ns to 300 ps, the excellent agreement between our analytical and numerical results allows to set at $I_{c0} = 50$ kW/cm² a threshold for the

intensity of the control laser above which the Doppler effect becomes negligible. In this regime of long pulse duration ($\delta\omega_{12} > \delta\omega_p$) the condition $\Omega_{c0} > 2.0\delta\omega_{12}$ (corresponding to $I_{c0} > 50$ kW/cm^2) guarantees that everywhere in the cell Ω_c is more than one order of magnitude larger than $\delta\omega_p$.

The comparison between the analytical and the numerical results obtained for the second compression step, from 300 ps to 30 ps, shows that the qualitative conditions $\Omega_c \gg \delta\omega_p$ and $\Omega_c \gg \delta\omega_{12}$ (both required in order to apply the strong-field analysis of Sec. III) lead to quantitatively different requirements at the cell input. In fact, while the condition $\Omega_{c0} > 2.0\delta\omega_{12}$ is confirmed to be sufficient for the Doppler effect to be neglected, a more stringent condition on the ratio $\Omega_{c0}/\delta\omega_{p0}$ is required by the compression dynamics in this regime of short pulse duration.

Even though obtained in our particular injection scheme, we deem these results of some general validity, and we believe that they provide very useful informations for the design of experiments aiming to the control of the temporal duration of short wavelength laser pulses.

ACKNOWLEDGMENTS

[1] S. E. Harris, Phys. Today **50** (7), 36 (1997).

[2] A. Kasapi, M. Jain, G. Y. Yin, and S. E. Harris, Phys. Rev. Lett. **74**, 2447 (1995).

[3] P. W. Milonni, J. Phys. B **35**, R31 (2002).

[4] S. E. Harris, J. E. Field, and A. Imamoglu, Phys. Rev. Lett. **64**, 1107 (1990); R. Buffa, S. Cavalieri, and M. V. Tognetti, *ibid.* **93**, 129401 (2004); Phys. Rev. A **72**, 037801 (2005).

[5] D. F. Phillips, A. Fleischhauer, A. Mair, R. L. Walsworth, and M. D. Lukin, Phys. Rev. Lett. **86**, 783 (2001).

[6] G. Nikoghosyan, Eur. Phys. J. D **36**, 119 (2005).

[7] M. Fleischhauer and M. D. Lukin, Phys. Rev. A **65**, 022314 (2002).

[8] A. S. Zibrov, A. B. Matsko, O. Kocharovskaya, Y. V. Rostovtsev, G. R. Welch, and M. O. Scully, Phys. Rev. Lett. **88**, 103601 (2002).

[9] M. D. Lukin, Rev. Mod. Phys. **75**, 457 (2003).

[10] M. Fleischhauer, A. Imamoglu, and J. P. Marangos, Rev. Mod. Phys. **77**, 633 (2005).

[11] Chien Liu, Z. Dutton, C. H. Berhoozi, and M. V. Hau, Nature (London) **409**, 490 (2001).

[12] R. Buffa, S. Cavalieri, and M. V. Tognetti, Phys. Rev. A **69**, 033815 (2004).

[13] R. Buffa, S. Cavalieri, L. Fini, E. Sali, and M. V. Tognetti, Opt. Commun. **264**, 471 (2006).

[14] V. G. Arkhipkin and I. V. Timofeev, Phys. Rev. A **73**, 025803 (2006).

[15] R. Buffa, S. Cavalieri, and M. V. Tognetti, Opt. Lett. **29**, 2432 (2004).